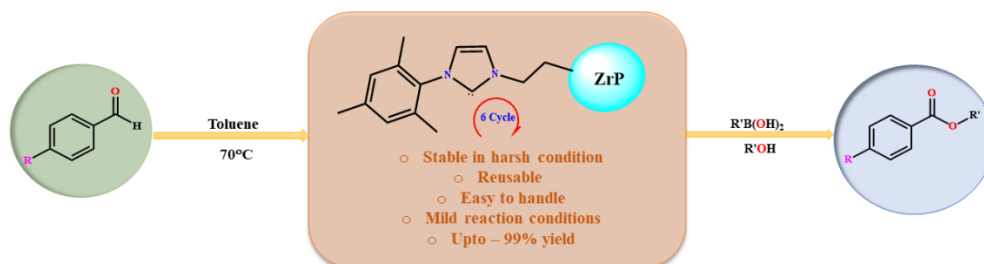**Chapter 3**

Imidazolium functionalized zirconium(IV) organophosphonate framework: An efficient heterogenous organocatalyst for aerobic esterification of aldehydes

Abstract: A simple and facile approach to prepare a layered Zr(IV) phosphonate with covalently anchored imidazolium functionality is developed. Reaction of phosphonic acid functionalized imidazolium salt with $ZrOCl_2.2H_2O$ gave quantitative yield of the desired Zr(IV) phosphonate with dangling imidazolium group. The title compound is characterized by elemental analysis, FT-IR, TGA, powder-X-ray diffraction, solid state MAS ^{13}C and ^{31}P NMR, X-ray photoelectron spectroscopy, energy dispersive X-ray spectroscopy and FESEM. The Zr(IV) phosphonate framework showed good catalytic activity in esterification of benzaldehyde with both aryl boronic acid and alcohols. The catalyst can be recycled up to six times in both the esterification reaction without any significant change in catalytic efficacy. Further, powder X-ray diffraction and FT-IR studies confirm the integrity of the catalyst recovered after the sixth catalytic cycle.

3.1. Introduction

N-heterocyclic carbenes (NHCs) have emerged as potent and powerful class of organocatalysts in a wide assortment of important organic transformations [1-6]. This diverse organocatalytic behaviour can be primarily attributed to the unique nucleophilicity of the carbene carbon atom and its concomitant propensity to attack carbon electrophiles. An enaminol intermediate known as Breslow intermediate formed upon nucleophilic attack of NHC carbon centre on an aldehydic carbon atom is relevant in such organocatalytic reactions [7-8]. The umpolung of carbonyl carbon upon formation of Breslow intermediate facilitated many reactions such as benzoin condensation, Stetter reaction etc. Apart from that the NHCs have also found application as organocatalysts in esterification of benzaldehyde with alcohol or boronic acids in presence of molecular oxygen or even atmospheric oxygen. NHC catalysed esterification of aldehydes with nucleophilic reagents containing alkyl halides, aziridines and hydroxyl compounds, etc. are well documented in literature [9-23].

Catalytic residual contamination left by homogeneous catalyst remains a major concern in pharmaceuticals as well as fine chemical industry. In this regard, development of heterogeneous catalytic systems with catalytic activity comparable to homogeneous catalyst, but augmented recyclability is an utmost requirement [24]. Thus, heterogeneous catalytic systems fabricated by anchoring catalytically active fragments on an inert solid support has evolved as prolific alternative to using homogenous catalysts. Organic polymer materials are widely used as solid support for imidazolium salts and plethora of heterogeneous organocatalytic systems exploiting the corresponding heterogenous NHCs have been designed accordingly [25-39]. Recently, metal organic frameworks (MOFs) have emerged as versatile support to accommodate catalytically active fragments and thereby design superior heterogenous catalytic systems. The porous, crystalline and inorganic-organic hybrid nature of MOFs provide endless opportunities to engineer catalyst microenvironment and thereby design heterogenous catalyst with unparallel turnover numbers [40]. Nevertheless, a vast majority of MOFs so far used as catalyst support are typically fabricated by employing carboxylate-based linkers [41-43]. The poor hydrolytic stability of such carboxylate based have remained a primary issue that needs to addressed for their application as catalyst under harsh conditions [44-46]. It is pertinent to note here that in comparison to carboxylate-based MOFs, layered high valent metal organophosphonates show far superior hydrolytic stability [47-48]. Thus, it is anticipated

that the recyclability and stability of heterogeneous catalysts can be enhanced by embedding catalytically active fragments on the surface of high valent metal phosphonate framework. Substituents on the organophosphonate ligand in layered metal organophosphonates protrude on both faces of the surface and thereby offer an easy route to integrate catalytically active fragments on metal phosphonate surfaces by employing suitably functionalized organophosphonate ligand [49]. The intrinsic layered structure of metal organophosphonates is thus expected to result a well-ordered and well-exposed arrangement of catalytically active fragments over the 2-dimensional solid support and thereby facilitate better catalyst to substrate interaction and which in turn shall enhance catalytic efficacy. Despite these possibilities, heterogeneous catalyst using metal organophosphonate support are scarce. To the best of our knowledge only no previous studies have focused on investigating organocatalytic activity of organocatalytic fragments covalently anchored on a metal organophosphonate framework [50]. In the present work, we have developed an imidazolium group functionalized phosphonic acid and its reaction with $ZrOCl_2$ yielded a Zr(IV) phosphonate decorated with imidazolium fragments. The resulting material was characterized by employing analytical, spectroscopic, structural and microscopic techniques while its organocatalytic efficacy in esterification of benzaldehyde with both aryl boronic acid and alcohols were investigated.

3.2. Materials and Methods

Starting materials were purchased from commercial sources and used without further purification. Solvents were purified by conventional techniques and distilled prior to use. 3-(2-(diethoxyphosphoryl)ethyl)-1-mesityl-1H-imidazol-3-ium-bromide is prepared as described in Chapter 2. Scanning electron microscope and EDS were recorded on JSM 6390LV. The powder X-ray diffraction patterns were recorded on a Bruker AXS D8 Focus X-ray diffractometer instrument using a nickel filtered CuKα (0.15418 nm) radiation source and scintillation counter detector. Infrared spectra were recorded from 400 to 4000 cm^{-1} on Perkin Elmer Frontier MIR-FIR FT-IR spectrophotometer on as KBr diluted discs. Thermogravimetric analysis (TGA) was performed with the help of a thermal analyzer (Model TGA-50 and DSC-60, Shimadzu). The progress of the reaction was monitored by thin layered chromatography (TLC) using aluminium sheets with silica gel 60F254 (Merck). UV light was used as a visualising agent. NMR spectra were recorded on a JEOL JNM-ECS400 NMR spectrometer operating at 400 MHz and samples were dissolved in deuterated solvents. Chemical shifts were reported in parts per million

downfield of Me$_4$Si (TMS) as internal standard. X-ray photoelectron spectroscopic (XPS) analyses were performed in KRATOS Axis ultra DLD spectrometer using Al Kα (1486.6 eV) radiation source. Magic angle spinning NMR (MAS NMR) of ^{13}C and ^{31}P were recorded with AVANCE III 500WB spectrometer using adamantane (δ = 38 ppm) and H$_3$PO$_4$ (δ = 0 ppm) as references, respectively. GCMS were recorded in a PerkinElmer Clarus 680 GC/600C MS instrument.

3.3. Experimental Section

3.3.1. Synthesis of 1-mesityl-3-(2-phosphonoethyl)-1H-imidazol-3-ium chloride (**9**)

To 3-(2-(diethoxyphosphoryl)ethyl)-1-mesityl-1H-imidazol-3-ium-bromide (5.21 mmol, 2.25 g), 30 mL of 6 M HCl was added and the mixture was refluxed for 12 h. The resultant solution was cooled to room temperature. The acid from the mixture was evaporated in a water bath and the hydrolysed product was obtained as yellow liquid. Yield: 2.145 g (82 %); Elemental analysis % found (calculated for C$_{14}$H$_{20}$ClN$_2$O$_3$P): C: 50.73 % (50.84 %) H: 6.02 % (6.10 %) N: 8.39 % (8.47 %); FT-IR (KBr, cm^{-1}): υ 3400(b), 2292(m), 1630(m), 1568(w), 1449(w), 1202(s), 1016 (s), 852(w), 748(w), 644(w), 502 (w). ^{1}H NMR (400 MHz, D$_2$O, δ/ppm): 8.91 (1H, Im-H), 8.79 (1H, Im-H), 7.72 (1H, Ar-H), 7.61 (1H, Im-H), 7.46(1H, Ar-H), 7.05 (2H, Ar-CH$_2$), 2.28 (2H, P-CH$_2$), 2.24(3H, Ar-CH$_3$), 1.92 (6H, Ar-CH$_3$). ^{13}C (100 MHz, D$_2$O, δ/ppm): 141.48 (Im, N-C-N), 136.66 (C^{Ar}), 134.77 (C^{Ar}), 130.81 (C^{Ar}), 129.31 (C^{Ar}), 124.28 (Im, C), 123.13 (Im, C), 45.14, 28.56, 20.26, 16.47. ^{31}P NMR (D$_2$O, δ/ppm): 21.79.

3.3.2. Synthesis of [Zr(RPO$_3$)$_{1.32}$(OH)$_{1.36}$]Cl$_{1.32}$.nH$_2$O (**10**)

An equimolar amount of 1-mesityl-3-(2-phosphonoethyl)-1H-imidazol-3-ium chloride (2.7 mmol, 800 mg) and ZrOCl$_2$.8H$_2$O (2.7 mmol, 873 mg) was dissolved in water. The reaction mixture was heated at 70°C for 4 consecutive days. White amorphous solid was obtained which was collected by centrifugation after the reaction and washed several times with distilled water and finally oven dried in oven at 60°C. Yield: 0.25g (31.25 %). Elemental analysis % found (calculated for C$_{15.26}$H$_{27.71}$Cl$_{1.09}$N2$_{.18}$O$_{9.1}$P$_{1.09}$Zr): C 36.09 (36.67 %), H 4.53 (4.02 %), N 7.62(7.78 %), P 5.57 (8.60 %). FT-IR: (KBr, cm^{-1}): υ 3422(br),1635(s), 1549(m), 1204(m), 1035(s), 526(m). TGA (10 °C/minute under air): Temperature range (% weight loss): 100-282 °C (17.59 %); 282-336 °C (9.19 %).

3.3.3. Aerobic esterification of aromatic aldehydes with boronic acid

Aromatic aldehyde (0.65 mmol) was added to a suspension of boronic acid (0.5 mmol), **10** as catalyst (10 mol%) and caesium carbonate (0.75 mmol) in toluene (10 mL) at room temperature. The reaction mixture was refluxed at 70 ℃ under open atmosphere (in the presence of air) until the reaction was complete. The reaction was monitored by using thin layered chromatography (TLC). After completion of the reaction, the reaction mass was filtered through a pad of celite®, washed with ethyl acetate (10 mL) and dried over anhydrous Na_2SO_4. The solvent was evaporated under reduced pressure and the residue was purified through silica gel column using ethyl acetate/hexane mixture as an eluent. Percentage conversions were determined using GC-MS methods.

3.3.4. Aerobic esterification of aromatic aldehydes with alcohols

To a flame dried round bottom flask equipped with a magnetic stir, catalyst **10** (10 mol %), Cs_2CO_3 (0.17 mmol, 10 mol %) and toluene (10 ml) were added. The resultant reaction mixture was kept on stirring at room temperature for 45 minutes. Aromatic aldehyde (0.5 mmol) and alcohol (5.5 mmol) was added successively. The reaction was refluxed at 70 ℃ for 9 hours. The progress of the reaction was monitored by thin layered chromatography (TLC). After completion of the reaction the mixture was filtered using celite pad in a Buchner funnel. H_2O (3 x50 mL) was then added to the mixture and extracted with ethyl acetate (20 ml). The combined organic layers were dried over anhydrous Na_2SO_4. Toluene and ethyl acetate was then evaporated to give crude ester, which was purified by column chromatography to obtain pure esters. Percentage yields of aryl ester formed were determined using GC-MS.

3.3.5. Catalyst recyclability test

Catalytic reusability was conducted using 4-chloro benzaldehyde and phenyl boronic acid as standard reaction for the first esterification set and 4-chloro benzaldehyde and methanol for the second set of reaction under standardized reaction procedure. It was conducted by separation of the catalyst through centrifugation method followed by several washes with toluene after each catalytic cycle. Further the catalyst was dried at 60 °C for 12 h before reuse. The dried catalyst was reused for esterification reaction. The catalyst performance for five consecutive cycles was investigated using GC-MS.

3.4. Results and discussion

3.4.1. Synthesis and characterization of imidazolium functionalized phosphonic acid (9)

The synthetic approach towards preparation of imidazolium functionalized phosphonic acid, (1-mesityl-3-(2-phosphonoethyl)-1H-imidazol-3-ium chloride) ($RPO(OH)_2$) consists of two steps (Scheme 3.1). Initially, 1-(2,4,6-Trimethylphenyl)-1H-imidazole was prepared by following an established procedure [51]. Thereafter, reaction of equimolar amounts of 1-(2,4,6-Trimethylphenyl)-1H-imidazole and diethyl-2-bromoethyl phosphonate in tetrahydrofuran (THF) yielded the desired imidazolium functionalized phosphonate ester, $RPO(OC_2H_5)_2$ as described in Chapter 2 of this thesis. Subsequently, $RPO(OEt)_2$ (**5**) was hydrolyzed by addition of 6M HCl to obtain the desired imidazolium functionalized phosphonic acid, $RPO(OH)_2$ (**9**) in good yield. Elemental analysis, FT-IR and NMR studies are in good agreement with the proposed formulation of **9**.
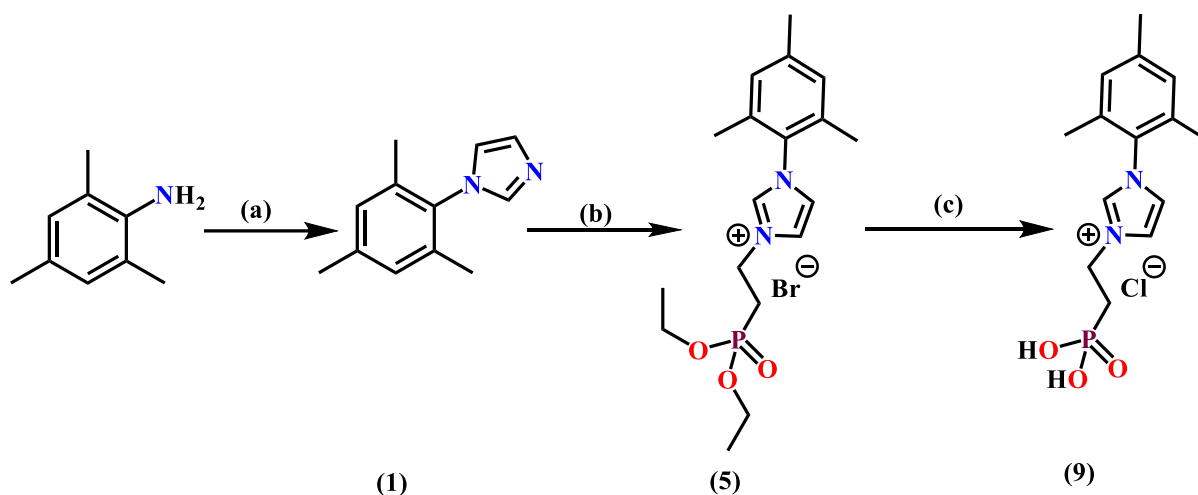
Scheme 3.1. Synthesis of **5** & **9**; conditions: (a) Glyoxal, NH_4Cl, HCHO, CH_3COOH, 18 hrs (reflux) (b) diethyl-2-bromoethyl phosphonate, THF (reflux); (c) 6 M HCl, reflux, 12 hrs

In the FT-IR spectrum of $RPO(OH)_2$ (**9**) showed all the relevant peaks as expected. Peak observed at 1630 cm^{-1} in the FT-IR spectrum of **9** corresponds to the C=N stretching vibration of the imine linkage of the imidazole functionality (Figure 3.1). Characteristic P=O and P-O stretching vibrations are observed as intense bands at 1202 cm^{-1} and 1016 cm^{-1}. Moreover, the broad peak observed at 2292 cm^{-1} can be assigned to the P-OH stretching vibration and confirms hydrolysis of the precursor phosphonate ester to the corresponding phosphonic acid, **9**.
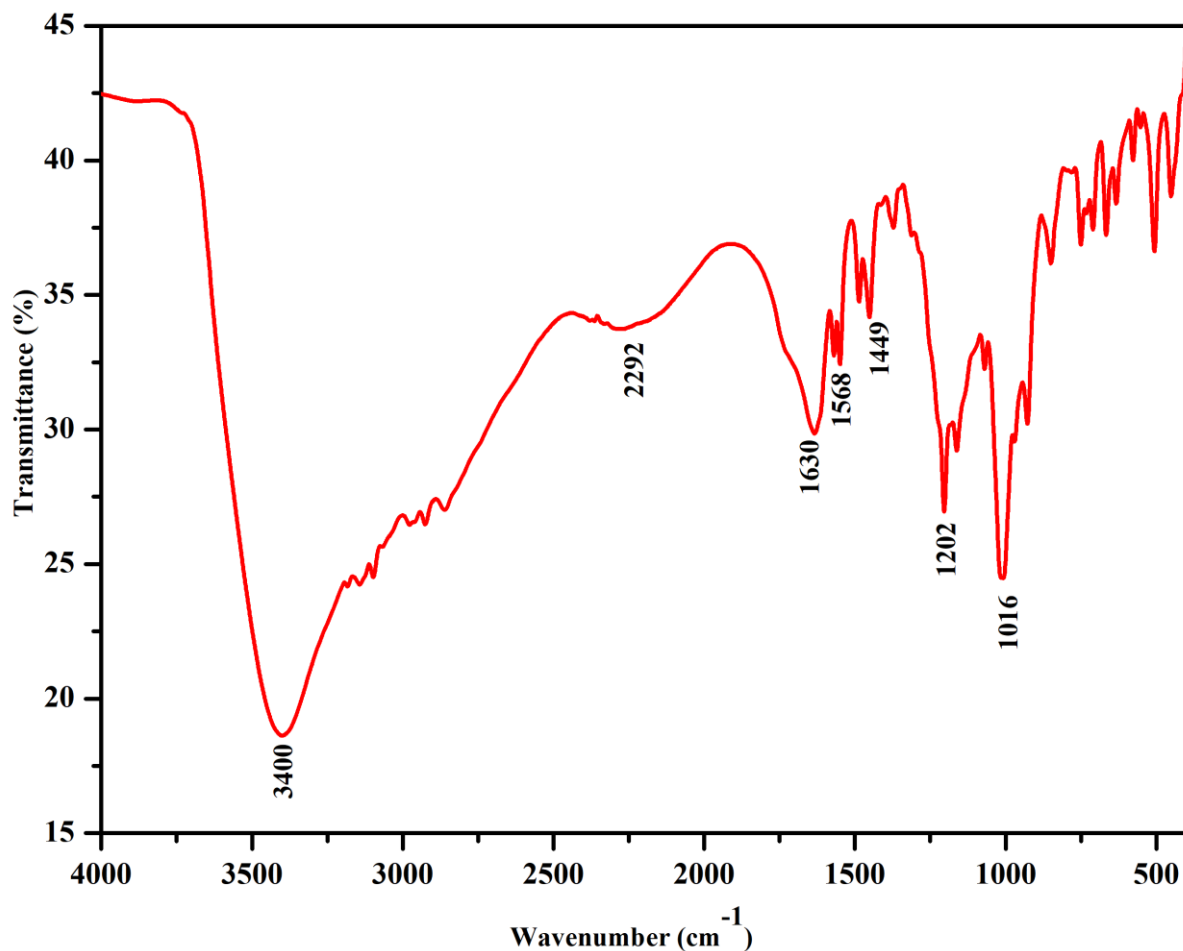
Figure 3.1. FT-IR spectrum of 1-mesityl-3-(2-phosphonoethyl)-1H-imidazol-3-ium chloride (**9**)

^{1}H NMR spectra of **9** show peaks for all constituent protons in expected regions and consistent with the proposed formula of the ligands (Figure 3.2). Chemical shift corresponding to the -CH$_3$ and -CH$_2$ fragments of the precursor phosphonate ethyl ester **5** were observed at 1.15 ppm and 3.97 ppm respectively (*vide supra*). Absence of any peak in this region of the ^{1}H NMR spectrum of **9** confirms the complete hydrolysis of the phosphonate ester group to the corresponding phosphonic acid. The CH$_3$ protons at ortho positions of mesityl group resonate at 1.92 ppm while peak for those at para position is observed at 2.24 ppm. Peak observed at 2.28 ppm can be assigned to protons of -CH$_2$ group attached to phosphorous atom. In the precursor phosphonate ester, **5** the protons of -CH$_2$ group attached to imidazole nitrogen are observed at 4.77 ppm and signal for these protons in the NMR spectrum of 9 are masked by the peak for residual protons in D$_2$O. Peaks corresponding to the aromatic protons present in the imidazolium ring of **9** are

observed at 8.91, 7.72 and 7.46 ppm while the two aromatic protons of mesityl group appear as singlet at 7.05 ppm.
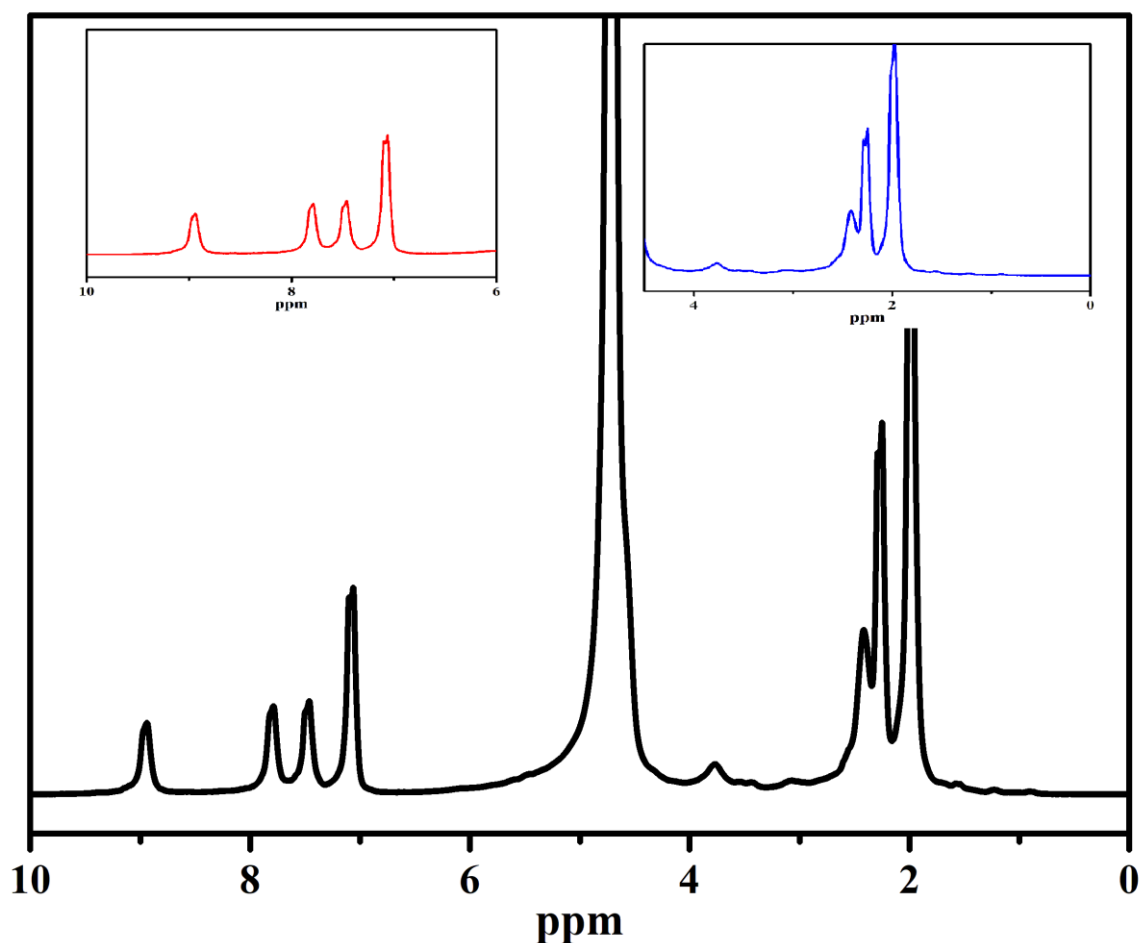

Figure 3.2. ^{1}H NMR spectrum of *1-mesityl-3-(2-phosphonoethyl)-1H-imidazol-3-ium chloride* (**9**)

^{13}C NMR spectra of **9** depicted in Figure 3.3 show peaks for all constituent carbon atoms in expected regions and consistent with the proposed formula of the phosphonic acid functionalized imidazolium salt. The characteristics signal for the imidazole C2 is observed at d 141.48 ppm. Peaks at 124.28 and 123.13 ppm can be attributed to the aromatic carbons of the imidazole group. The aromatic carbon atoms of mesityl ring resonate in the range (136.66-129.31) ppm while the signals at 20.26 and 16.47 ppm appear for the methyl carbons of the mesityl group. The characteristics resonances of carbons associated to the bridge ethylene group are observed at 45.14 and 28.56 ppm.
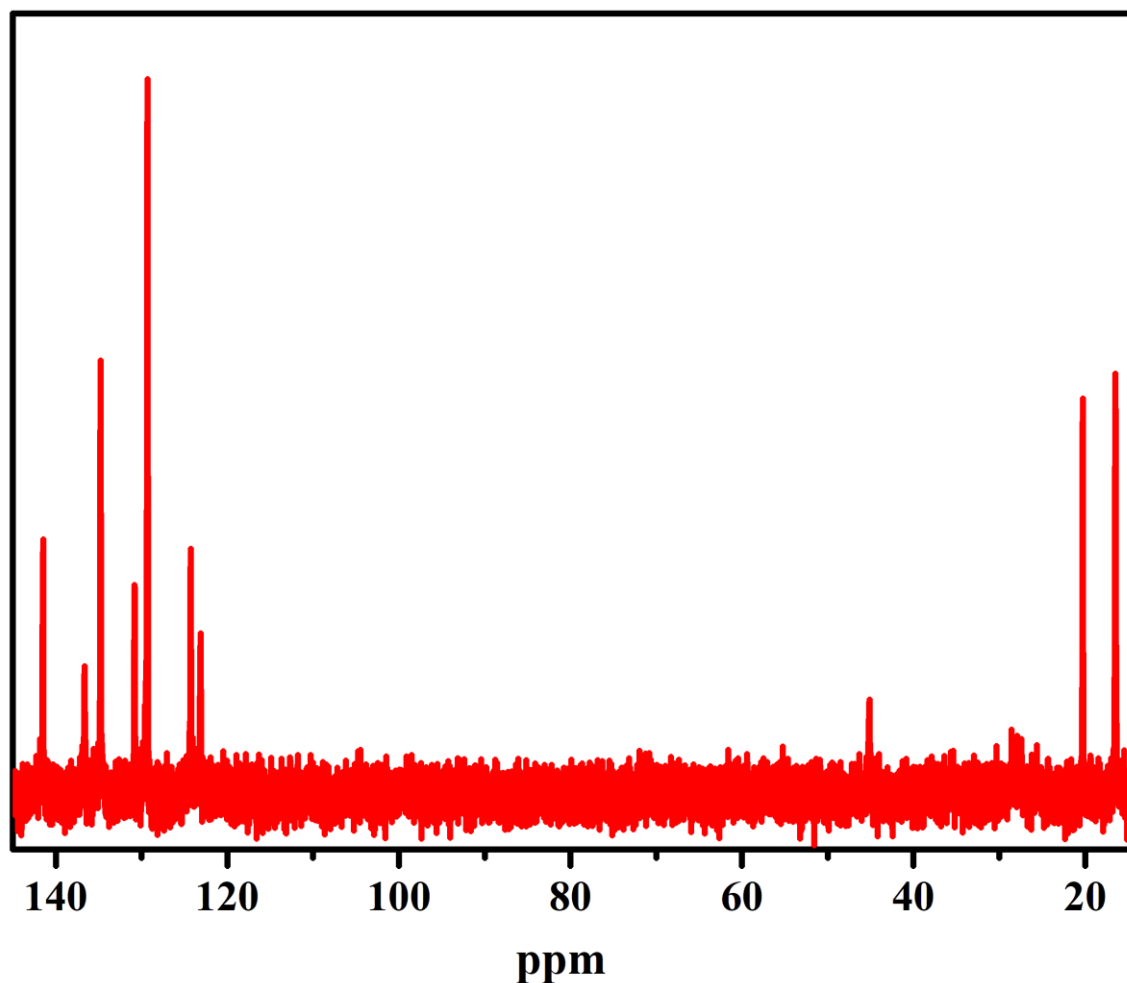
Figure 3.3. ^{13}C NMR spectrum of *1-mesityl-3-(2-phosphonoethyl)-1H-imidazol-3-ium chloride* (**9**)

^{31}P NMR is a versatile tool to probe the electronic environment of phosphorous in phosphonate esters and phosphonic acids as reasonable deviation in chemical shift is expected upon hydrolysis of phosphonate esters to corresponding phosphonic acid. While the ^{31}P NMR spectra of the precursor phosphonate ester **5** show a single resonance at 26.4 ppm, it shifts to 21.7 ppm upon hydrolysis to **9** which can be assigned to phosphorous atom of aliphatic phosphonic acids (Figure 3.4). These values are in good agreement with ^{31}P resonances observed in case of earlier reported aliphatic organophosphonic acids. Moreover, observation of only single resonance in the ^{31}P NMR spectrum of **9** establish the purity of this compound.
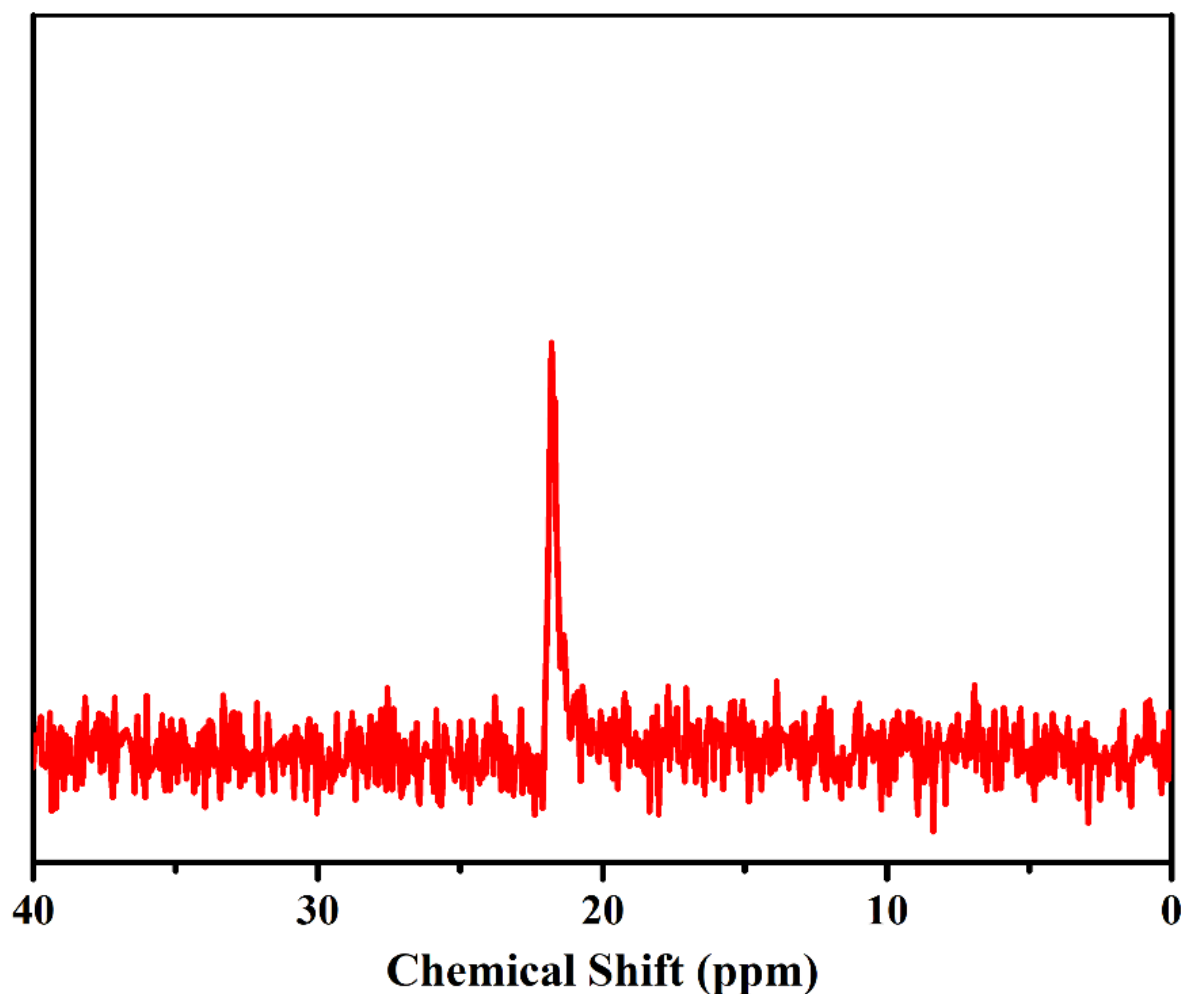
Figure 3.4. ^{31}P NMR spectrum of 1-mesityl-3-(2-phosphonoethyl)-1H-imidazol-3-ium chloride (**9**)

Due to the presence of polar hydrophilic –PO(OH)$_2$ groups, organophosphonic acids tend to aggregate in solution and produce discrete aggregates [52]. The association behavior of **9** in the gas phase was studied with the help of ESI-MS measurements in methanol under positive ionization mode. Interestingly, the spectra obtained not only exhibit an (M + 1)$^+$ ion peak, but also contain a peak corresponding to the formation of H-bonded (2M + 1)$^+$ aggregate in solution (Figure 3.5). The lack of aggregates of higher mass as observed in case of earlier reported phosphonic acids can be attributed to the presence of polar imidazolium substituents which prevent formation of higher aggregates due to dipor interactions.
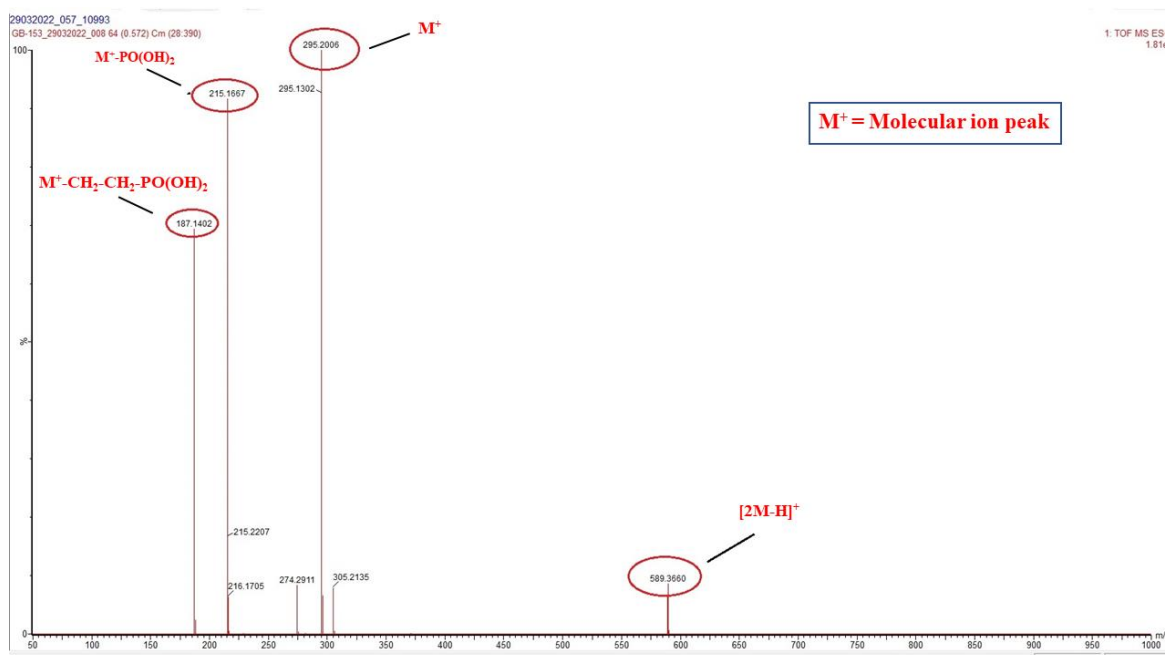
Figure 3.5. High Resolution Mass Spectrometric fragmentation pattern of *1-mesityl-3-(2-phosphonoethyl)-1H-imidazol-3-ium chloride* (**9**)

Thermogravimetric analysis of **9** was also carried out under N_2 atmosphere at a heating rate of 10 °C per minute. Compound **9** shows one distinct weight loss of 54.8% between temperature range 263.1-351.6 °C and this can be attributed to the loss of organic substituents (54.8 % theoretical weight loss) on the phosphonate ligand (Figure 3.6).
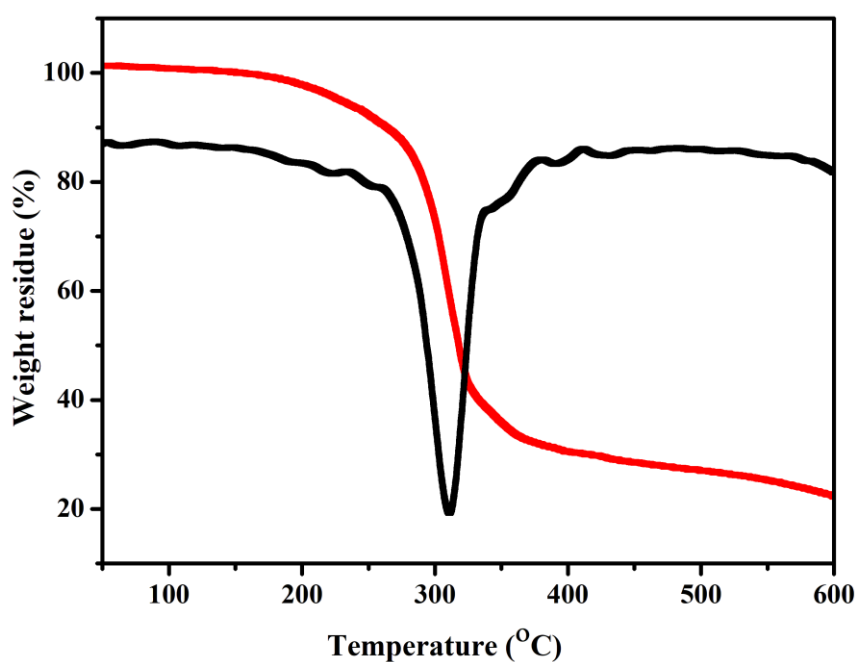

Figure 3.6. Thermo-gravimetric analysis pattern of **9** (Heating rate: 10 °C/minute; N_2 atmosphere)

*3.4.2. Synthesis and characterization of zirconium phosphonate framework (**10**)*

Organophosphonic acids undergo facile reaction with Zr(IV) salts under solvothermal conditions and result layered zirconium phosphonate framework where the organic substituents lie on both side of the layered framework. The layered structure of the resulting Zr(IV) phosphonate is retained irrespective of the nature of the organic substituent present. This offers unique opportunity to decorate the surface of Zr(IV) phosphonate with catalytically active groups by employing suitably functionalized organophosphonate ligand. In view of this, we carried out the reaction between the imidazolium functionalized phosphonic acid, **9** with $ZrOCl_2.8H_2O$ and isolated a new zirconium phosphonate framework with dangling aryl imidazolium functionality (Scheme 3.2). Analytical, spectroscopic and thermogravimetric analysis establish that the empirical formula of the present zirconium phosphonate framework is $[Zr(RPO_3)_{1.32}(OH)_{1.36}]Cl_{1.32}.5H_2O$ (**10**). Apart from that, structural and microscopic analysis of **10** is also carried out to establish its layered nature.
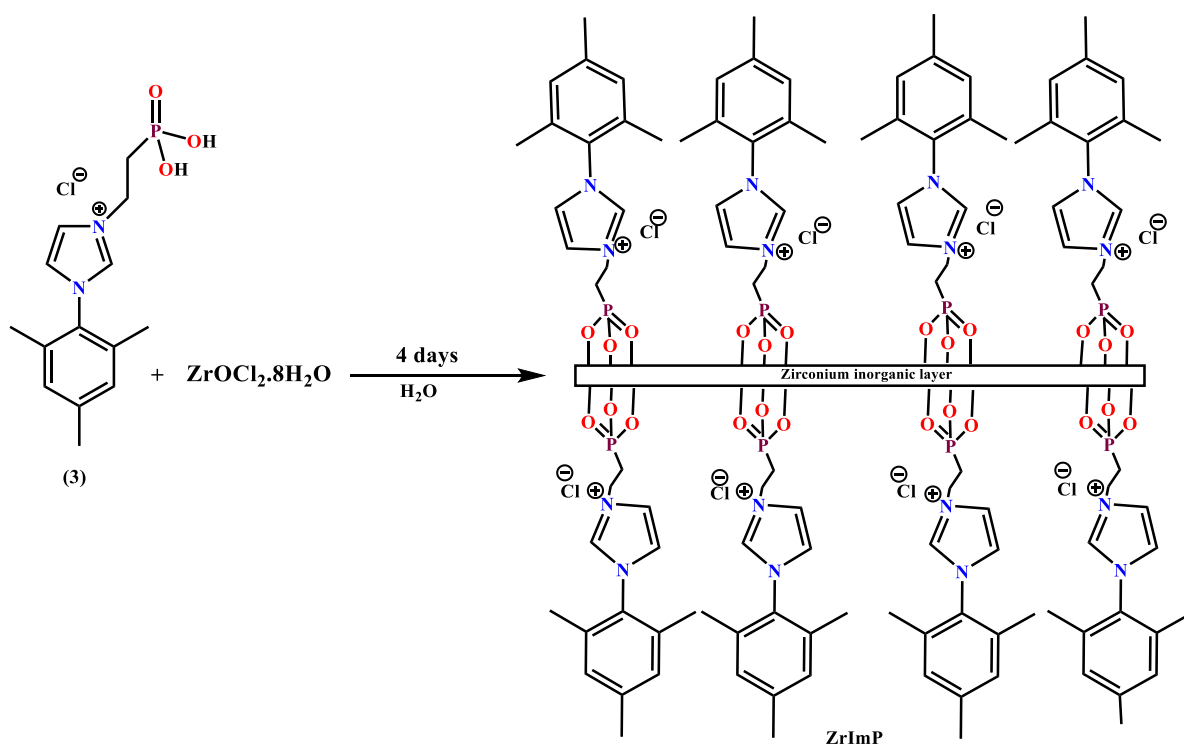
Scheme 3.2. Synthesis of **10**

Attempts to digest samples of **10** by using either concentration HNO_3 or aqua regia under heating failed due to its chemically robust nature. This prevented us from carrying out analytical measurements by using atomic adsorption or atomic emission spectroscopy.

However, both Energy-dispersive X-ray spectroscopy and X-ray photoelectron spectroscopic analysis of **10** reveal that the P/Zr atomic ratio is 1.32. Based on the available P/Zr atomic ratio, the empirical formula of **10** can be written as $[Zr(RPO_3)_{1.32}(OH)_{1.36}]Cl_{1.32}.nH_2O$.

The FT-IR spectrum of **10** shows an intense peak at 1035 cm^{-1}, that can be attributed to the Zr-O-P stretching vibrations and thus confirms the formation of the zirconium phosphonate framework (Figure 3.7). The P-OH stretching vibration observed at 2292 cm^{-1} in case of the precursor ligand, **9** is no longer visible in the FT-IR spectrum of **10** and this signifies formation of metal phosphonate linkage via deprotonation of the phosphonic acid ligand. Apart from that, all other relevant peaks of the parent imidazolium functionalized ligand, **9** are also observed in the FT-IR spectrum of **10**. The C=N stretching vibration of the imidazolium fragment in **10** appear as an intense signal at 1635 cm^{-1} which is minor deviation from that observed in case of **9**. This indicate that the electronic characteristics of the imidazolium fragment undergo no major changes upon coordination of the pendant phosphonic acid functionality with Zr(IV).
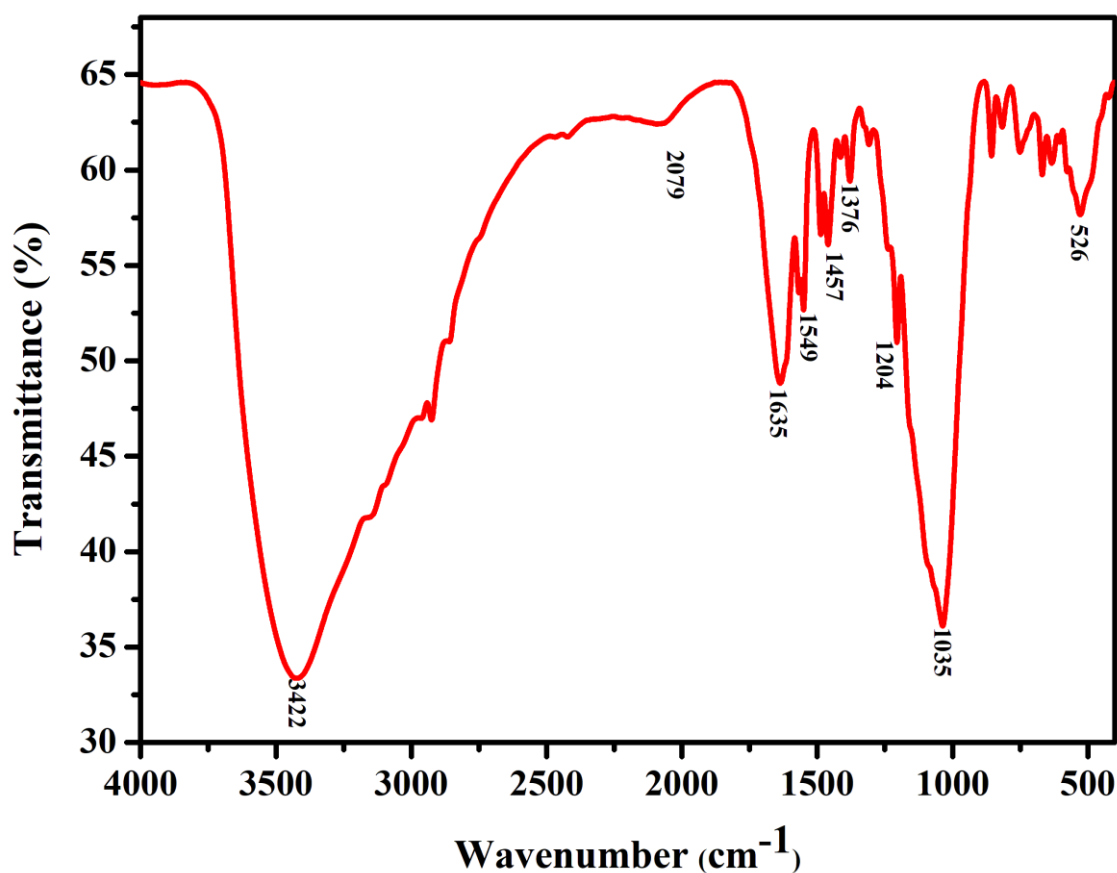

Figure 3.7. FT-IR Spectrum of **10**

The thermal stability of the compound **10** was investigated using thermogravimetric analysis (TGA) under N_2 atmosphere at a heating rate of 10 °C/minute. The TGA pattern shows an initial weight loss of 10 % on heating up to 152 °C and this can be attributed to the evaporation of the surface adsorbed and occluded water molecule in the framework. Thereafter, compound **10** remains stable on heating up to 282 °C after which another distinct weight loss of 12% is observed between 282-367 °C. Upon heating above 367 °C, steady and continuous weight loss is observed up to 700 °C (Figure 3.8). These weight losses can be attributed to the loss of organic substituents present on the phosphonate ligand which is in line with that observed in case of the free phosphonic acid ligand, **9**. Nevertheless, the loss of organic substituents in the free phosphonic acid ligand occur within a small temperature range of 263.1-351.6 °C while in case of the zirconium phosphonate framework, **10** the loss of organic substituents occur in a slow and stepwise manner which continue till 700 °C, the highest temperature under measurement. Thus, incorporation of the ligand into the zirconium phosphonate framework augment its thermal stability to some extent.
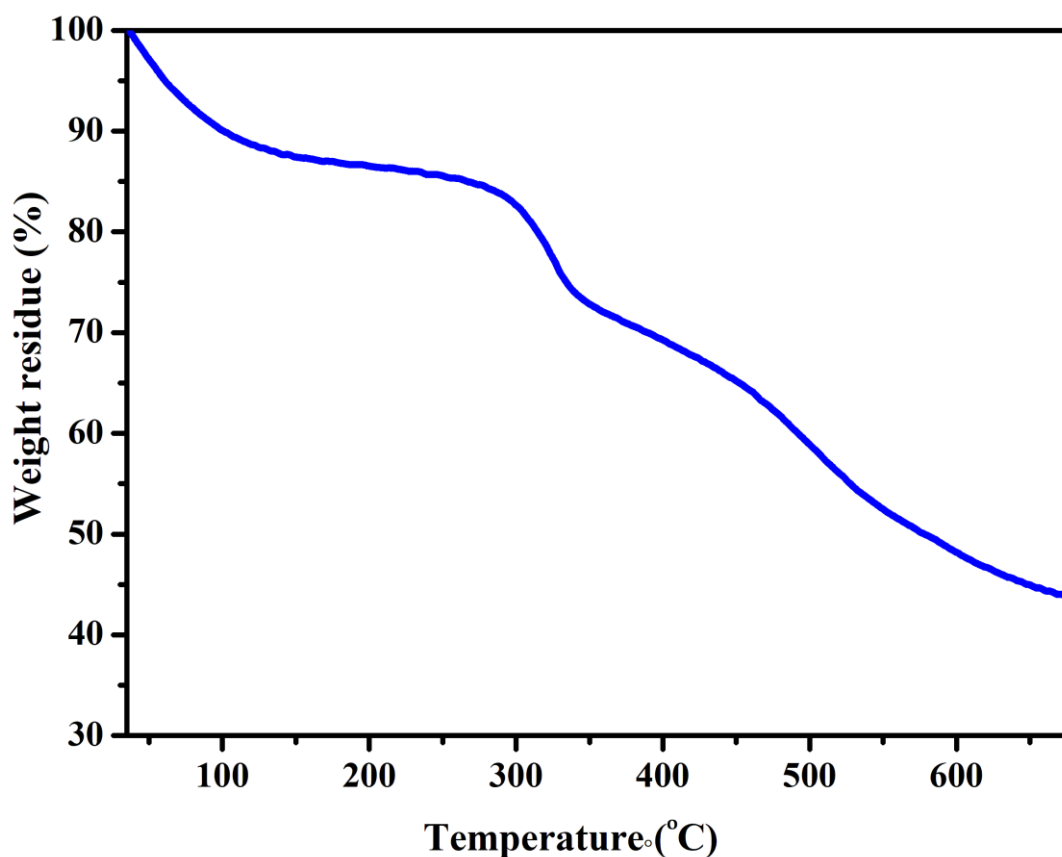

Figure 3.8. Thermo-gravimetric analysis pattern of **10** (Heating rate: 10 °C/minute; N_2 atmosphere)

The powder X-ray diffraction pattern of **10** is characteristic of layered Zr(IV) organophosphonate framework. Peak observed at $2\theta = 4.34°$ correspond to *d*-spacing of 20.40 Å (Figure 3.9). The observed interlayer distance is considerably high as compared to earlier reported zirconium organophosphonates. This can be attributed to the electrostatic and van-der Waal repulsion between the layers due to the presence of dangling aryl imidazolium groups on the surface of the layered zirconium phosphonate.
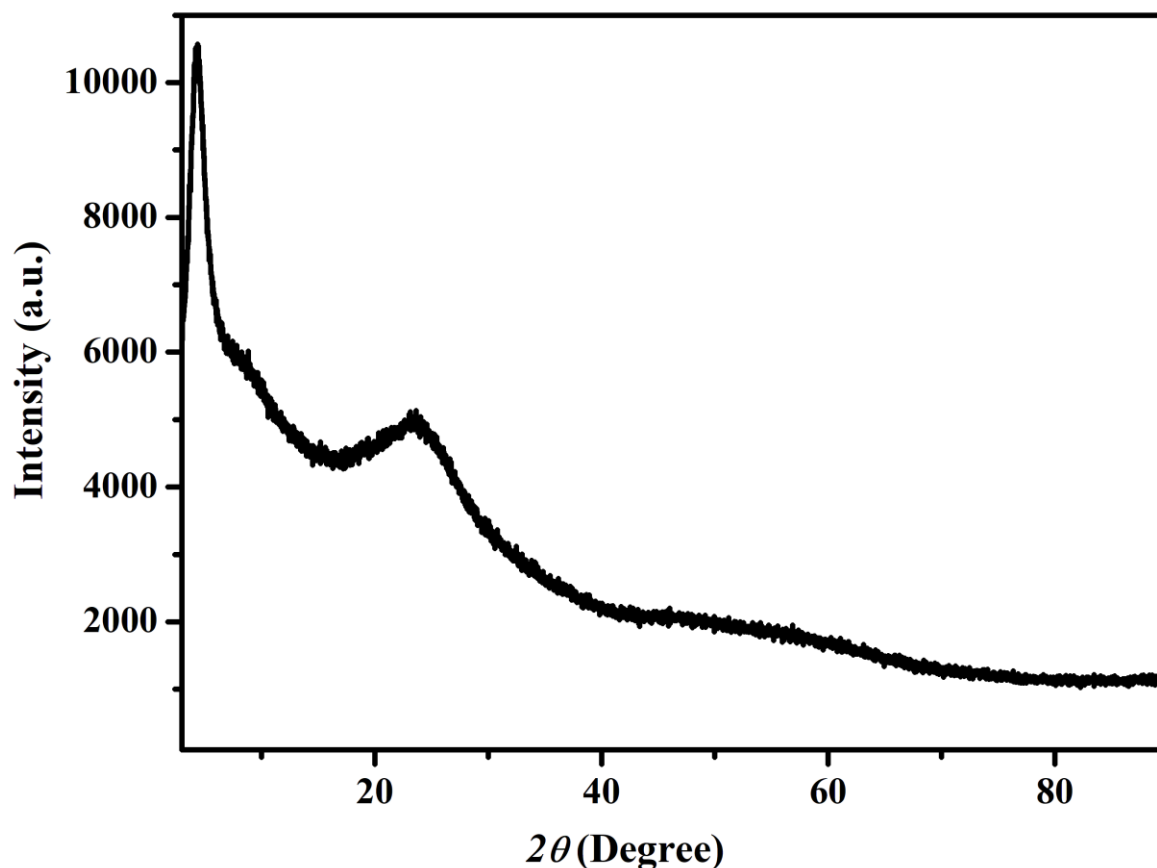

Figure 3.9. Powder X-ray diffraction pattern of **10**

^{13}C CP MAS NMR spectrum of **10** shows all the characteristic peaks for constituent carbon atoms in the organophosphonate ligand thereby established the integrity of the Organophosphonic acid precursor upon complexation with zirconium(IV) (Figure 3.10). Peaks observed at δ 18.0 & 29.6 ppm can be attributed to the methyl carbon atoms of mesityl group. Resonances for -CH$_2$ carbon atoms are observed at δ 31.4 ppm and 40.4 ppm. Peaks observed between δ 124.6-135.5 are the characteristic peaks of aromatic carbon atoms in the mesitylene group and the imidazolium ring.
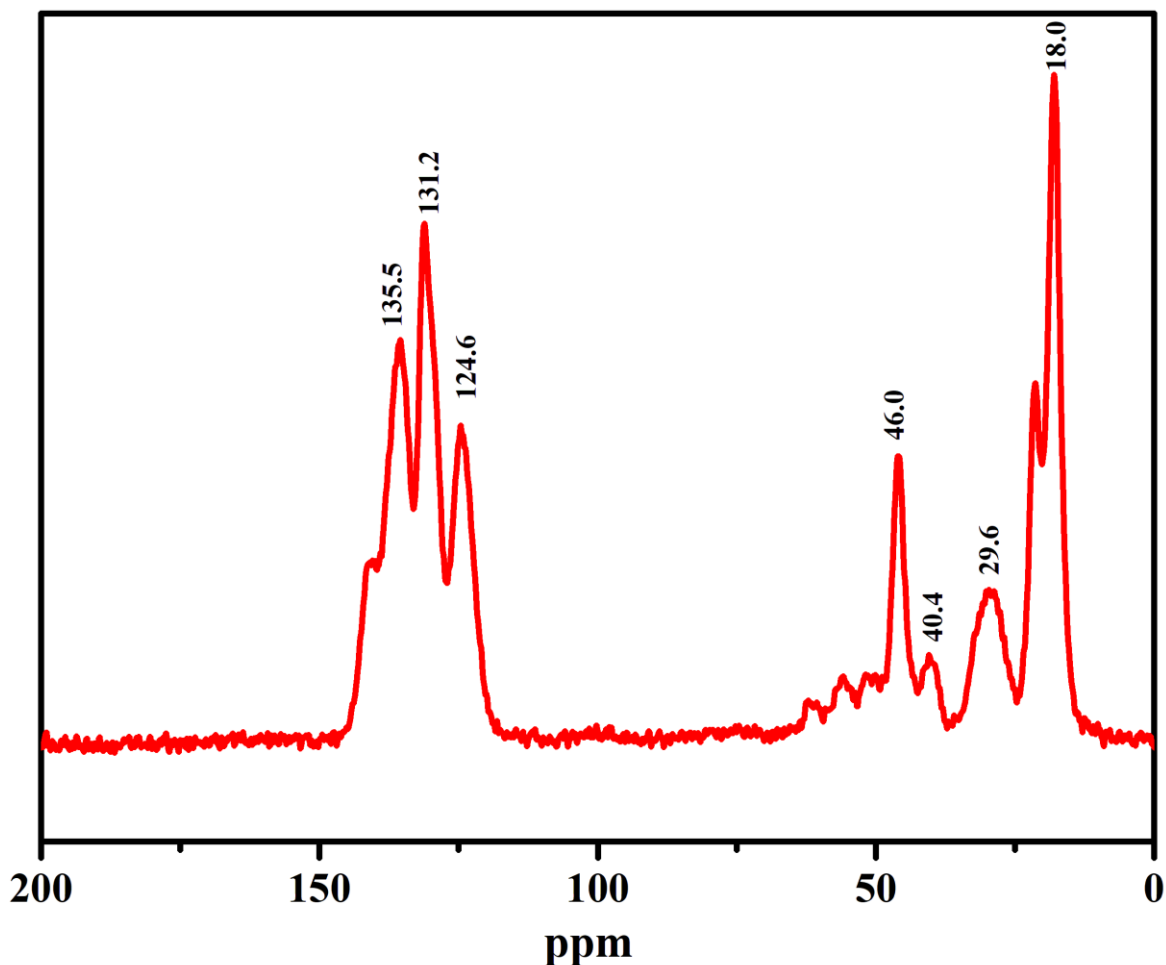
Figure 3.10. ^{13}C CP MAS NMR spectra of **10**

The chemical shift of phosphorous in phophonates is remarkably sensitive to surrounding environment and therefore ^{31}P MAS NMR can be used as a probe to investigate the nature of interaction of phoshonate group to the zirconium ion (Figure 3.11). ^{31}P MAS NMR spectrum of **10** shows two peaks at δ 2.52 and 7.80 ppm and this clearly reveals that the phosphonate ligands in **10** are coordinated to Zr(IV) ions in two distinct coordination modes. ^{31}P MAS NMR studies on earlier reported Zr(IV) alkylphosphonates with dangling imidazolium fragments show single resonance at ~5.7 ppm [49]. In principle, the three oxygen atoms of phosphonate ligand can bridge a total of nine metal centers and therefore phosphonate ligands are prone to show several coordination modes in metal phosphonates prepared by using soft chemical routes. Deconvolution of the ^{31}P NMR spectrum show that the ratio of peaks at 7.80 and 2.52 ppm is 94:6. Thus, six percent of the phosphonate ligands present in **10** show higher denticity as compared to the remaining ninety four percent phosphonate ligands. Spinning sidebands are seen either side of ^{31}P MAS NMR and their low intensity implies that the chemical shift anisotropy is small [53].
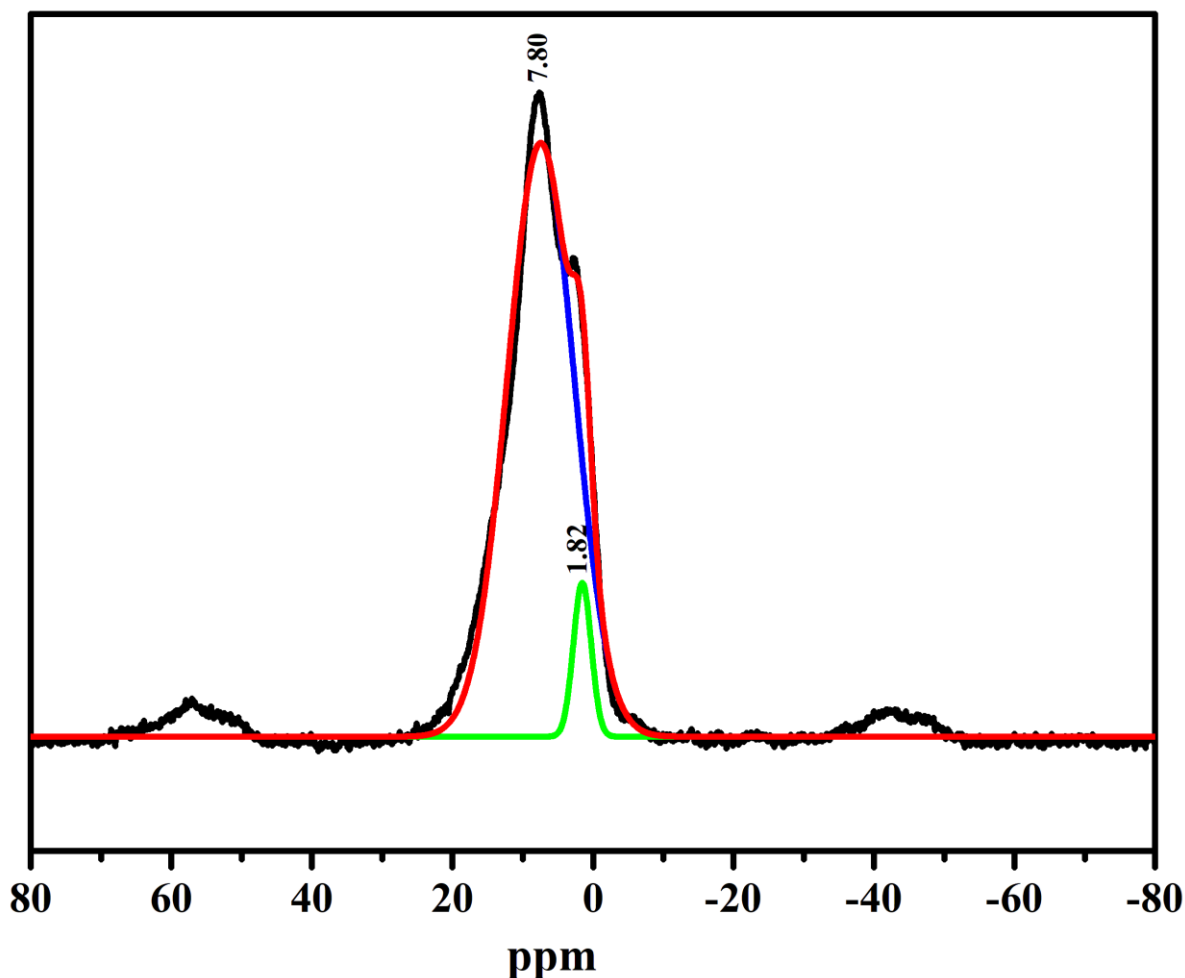
Figure 3.11. ^{31}P MAS NMR spectra of **10**

X-ray photoelectron spectroscopy (XPS) spectrum of **10** for all relevant regions are depicted in Figure 3.12 and characteristics peaks of all the constituent elements present in the zirconium phosphonate framework are observed in expected binding energy regions. Peaks corresponding to $3d_{5/2}$ and $3d_{3/2}$ electrons of Zr(IV) appeared at 182.7 eV and 185.1 eV respectively whereas $3p_{3/2}$ and $3p_{1/2}$ electrons of tetravalent zirconium are observed at 333.5 and 337.5 eV respectively. Peaks observed at 132.85 eV and 133.72 eV can respectively be assigned to $2p_{3/2}$ and $2p_{1/2}$ electrons of pentavalent phosphorus. Peaks at 284.67 eV and 286.05 eV in the deconvoluted C1s XPS spectrum can be attributed to C=C/C-C and C-N bonds respectively. Accordingly, the peaks at 401.43 eV and 399.36 eV from the deconvoluted N1s spectrum corresponds to C=N and C-N bonds respectively. Further, the % compositon of different elements obtained from XPS analysis of **10** agree well with the proposed formulation of the zirconium phosphonate framework.
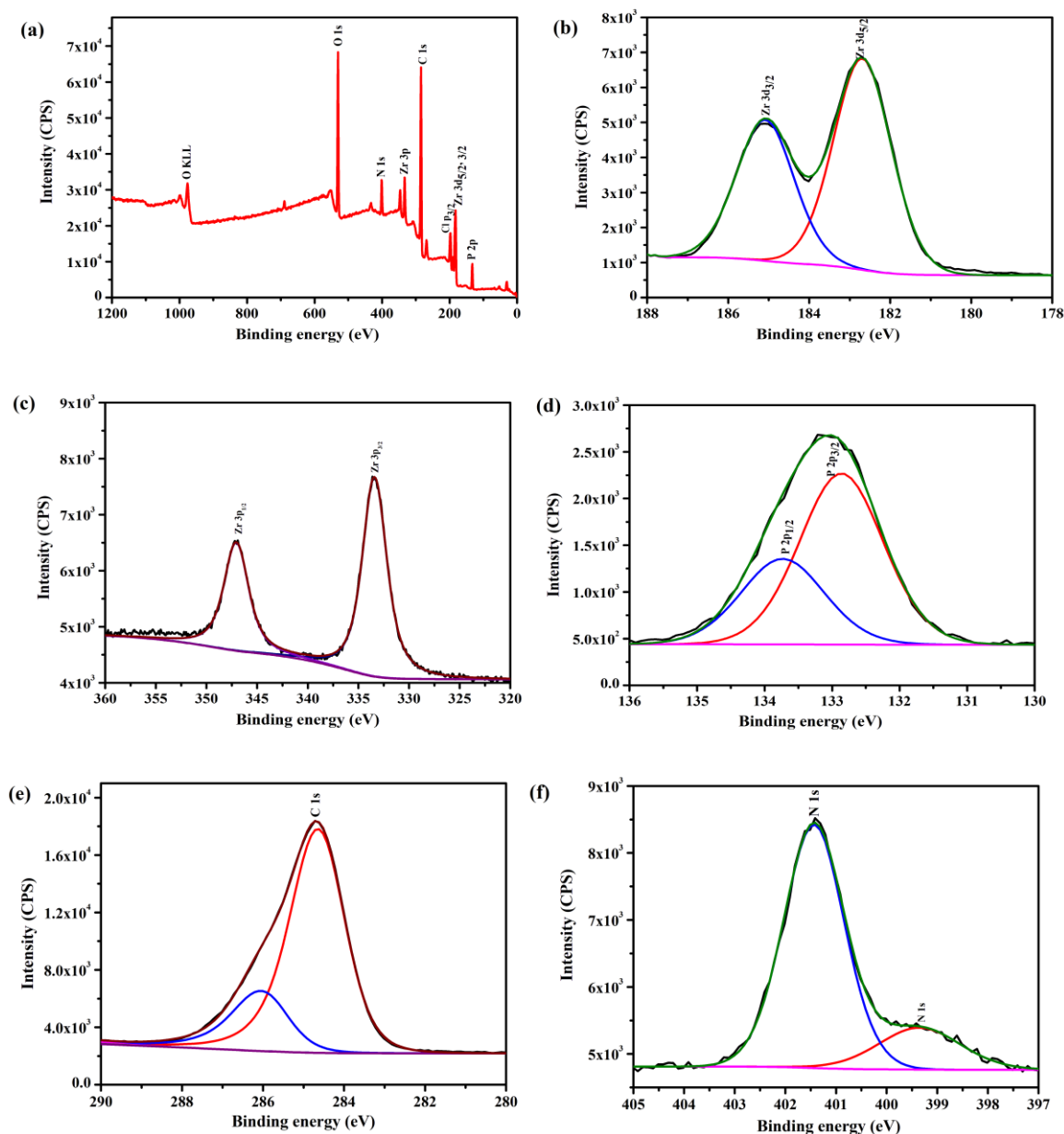
Figure 3.12. X-ray photoelectron spectra of 10 (a) entire range (b) Zr 3d range (c) Zr 3p range (d) P 2p range (e) C 1s range (f) N 1s range

Surface morphology of **10** was visualized by using scanning electron microscopic technique. The images revealed that the compound forms thin and highly stacked layers of flakes of non-uniform size. Such morphology is typical of layered metal organophosphonates with long hydrocarbon substituents. Elemental mapping was performed by energy dispersive X-ray spectroscopy reveals the presence of all the constituent elements of the framework (Figure 3.13).
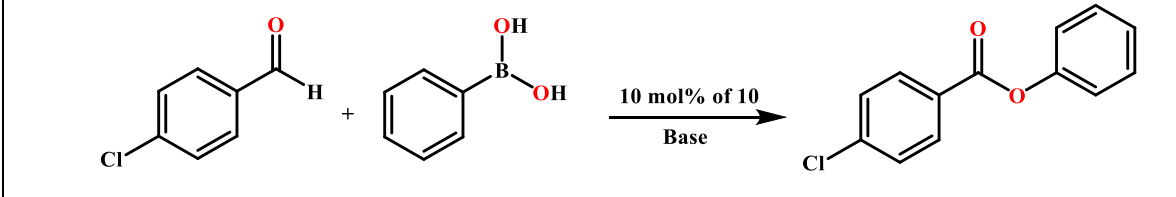
Figure 3.13. SEM image of **10**

3.4.3. Catalytic esterification of benzaldehyde with aryl boronic acid or alcohols

The catalytic activity of **10** in esterification reaction of benzaldehyde with two different substrates e.g. phenyl boronic acid and alcohol are studied. Initially optimization of reactions c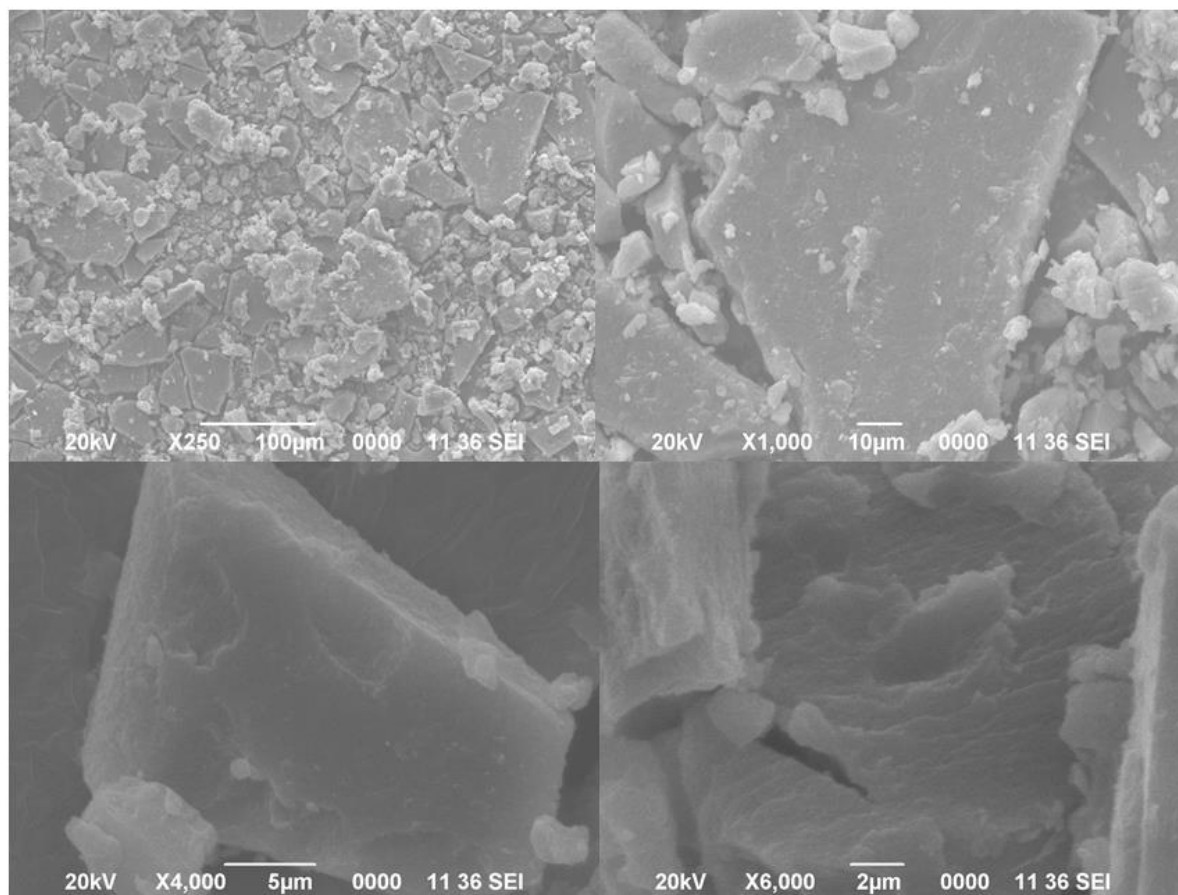onditions e.g. temperature, time and solvent were carried out for both the reaction by using 10 mol% of **10** as catalyst. First optimization studies on esterification of benzaldehyde with aryl boronic acid were carried out by using para-chlorobenzaldehyde as model substrate (Table 3.1). The reaction did not proceed when carried out below 40 °C and 94% yield of the aryl ester was obtained when heated at 90 °C for 12 hours. The optimum reaction temperature and time giving best yield was found to be 70 °C for 12 hours. Cs_2CO_3 was found to give better yield of the ester as compared to other bases investigated while the reaction did not proceed when K_2CO_3 or $NaHCO_3$ were used as bases. Optimization of solvent was also carried out and toluene give the best yield while very poor yields were obtained in $CHCl_3$ or 1,4-dioxane.

Table 3.1. Optimization of reaction condition for **10** catalysed esterification of benzaldehyde with phenyl boronic acid


Sl. No.	Time (h)	Temperature (°C)	Base (10 mol %)	Solvent	% Yield
1.	1	rt	Cs_2CO_3	Toluene	No reaction
2.	12	30	Cs_2CO_3	Toluene	No reaction
3.	12	40	Cs_2CO_3	Toluene	30
4.	12	50	Cs_2CO_3	Toluene	45
5.	12	60	Cs_2CO_3	Toluene	72
6.	12	80	Cs_2CO_3	Toluene	92
7.	12	90	Cs_2CO_3	Toluene	94
8.	1	70	Cs_2CO_3	Toluene	No reaction
9.	2	70	Cs_2CO_3	Toluene	Trace amount
10.	5	70	Cs_2CO_3	Toluene	20
11.	7	70	Cs_2CO_3	Toluene	35
12.	9	70	Cs_2CO_3	Toluene	53
13.	10	70	Cs_2CO_3	Toluene	65
14.	11	70	Cs_2CO_3	Toluene	84
15.	**12**	**70**	**Cs_2CO_3**	**Toluene**	**90**
16.	13	70	Cs_2CO_3	Toluene	91
17.	12	70	K_2CO_3	Toluene	trace
18.	12	70	DBU	Toluene	30
19.	12	70	$NaHCO_3$	Toluene	trace
20.	12	70	Cs_2CO_3	THF	77
21.	12	70	Cs_2CO_3	CH_3CN	33
22.	12	70	Cs_2CO_3	1,4-Dioxane	15
23.	12	70	Cs_2CO_3	$CHCl_3$	10

Yields of corresponding aryl esters formed during the reaction of different p-substituted aldehyde with phenyl boronic acid under the above optimized conditions were investigated. It was observed that out of the three p-halobenzaldehydes investigated, p-chloro benzaldehyde gives the highest yield of 90% followed by para-fluoro and then para-bromo benzaldehyde with 78% and 75% yields respectively (Table 3.2). High conversion is observed when strongly electron withdrawing substituents are present on the benzaldehyde. Thus, esterification of p-nitro benzaldehyde with phenyl boronic acid catalysed by **10** give 97% yield of the corresponding aryl ester while relatively poor yield

was observed in case of 4-methyl benzaldehyde. Surprisingly, the reaction did not proceed even after 12 hours in case of 4-hydroxy benzaldehyde.

Table 3.2. Optimization of esterification reaction of p-substituted benzaldehydes with phenyl boronic acid
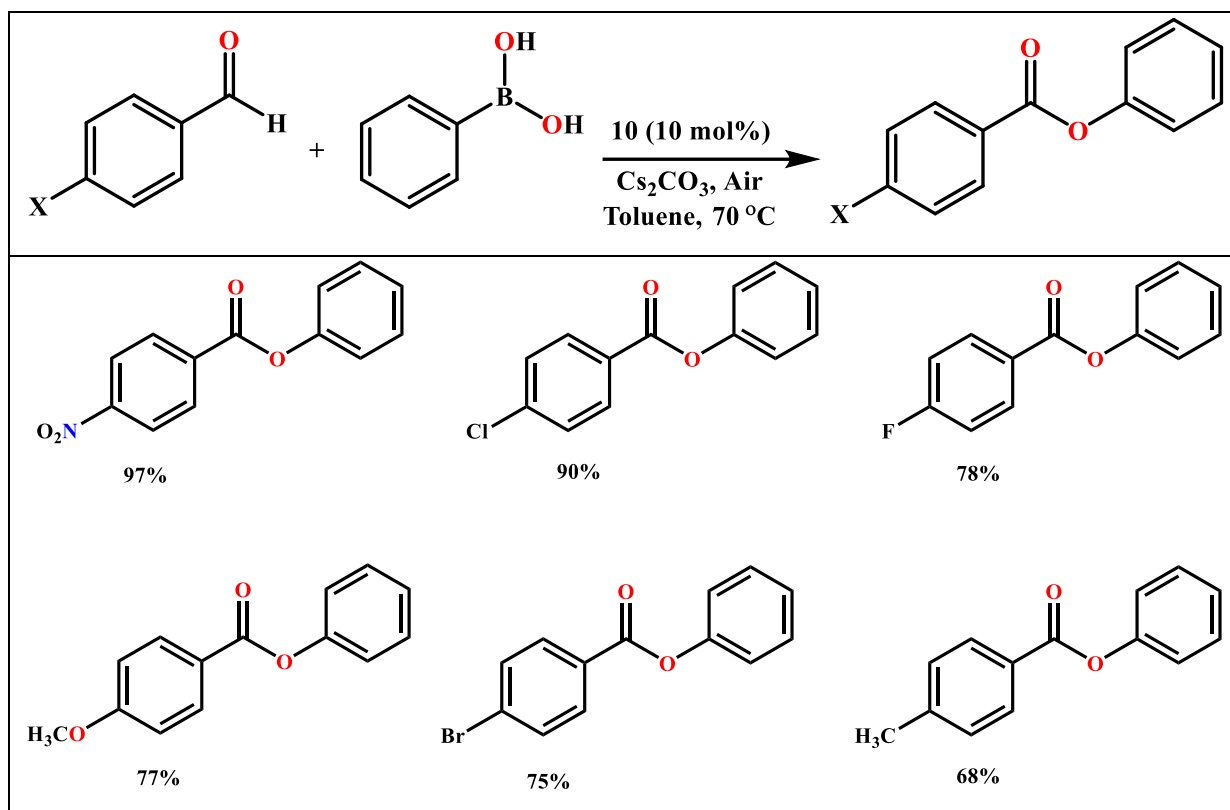
Good catalytic efficacy of **10** in esterification of p-substitute benzaldehyde with phenyl boronic acid led us to explore its catalytic efficacy in a related esterification reaction of substituted benzaldehyde with aliphatic alcohols. To establish the optimized reaction conditions of this esterification reaction, 4-nitrobenzaldehyde and methanol were taken as model substrates using 10 mol% of **10** as catalyst (Table 3.3). As observed in case of the esterification reaction of substituted benzaldehyde with aryl boronic acid, in this case also the reaction did not proceed at temperatures below 50 °C. The optimum reaction temperature was found to be 70 °C for a reaction time of 9 hours in toluene medium using Cs_2CO_3 as the base. The yield of the aryl ester was found to be very low when K_2CO_3 or $NaHCO_3$ were used as base. Moreover, polar hydrophilic solvents *e.g.* CH_3CN, 1,4-dioxane afforded relatively poor yields while poor yields observed when THF or $CHCl_3$ were used as solvents can also be attributed to low reaction temperatures.

Table 3.3. Optimization of reaction conditions of **10** catalysed esterification of benzaldehydes with aliphatic alcohols
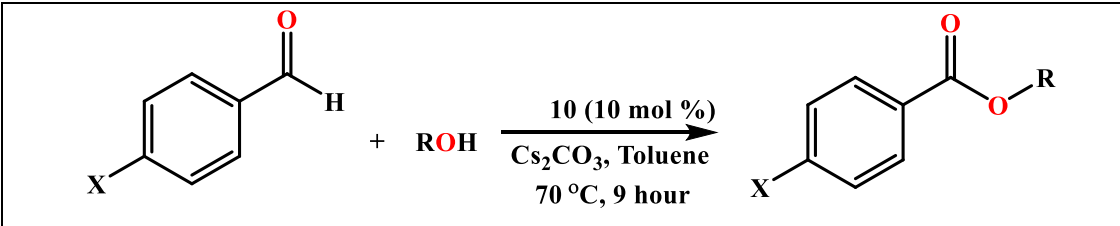

Sl. No.	Time (h)	Temperature (°C)	Base (10 mol %)	Solvent	% Yield
1.	1	rt	Cs_2CO_3	Toluene	No reaction
2.	9	30	Cs_2CO_3	Toluene	No reaction
3.	9	40	Cs_2CO_3	Toluene	No reaction
4.	9	50	Cs_2CO_3	Toluene	30
5.	9	60	Cs_2CO_3	Toluene	70
6.	**9**	**70**	**Cs_2CO_3**	**Toluene**	**99**
7.	9	80	Cs_2CO_3	Toluene	99
8.	1	70	Cs_2CO_3	Toluene	No reaction
9.	3	70	Cs_2CO_3	Toluene	10
10.	5	70	Cs_2CO_3	Toluene	35
11.	7	70	Cs_2CO_3	Toluene	70
12.	11	70	Cs_2CO_3	Toluene	99
13.	9	70	K_2CO_3	Toluene	15
14.	9	70	DBU	Toluene	20
15.	9	70	$NaHCO_3$	Toluene	10
16.	9	66	Cs_2CO_3	THF	84
17.	9	70	Cs_2CO_3	CH_3CN	45
18.	9	70	Cs_2CO_3	1,4-Dioxane	21
19.	9	61	Cs_2CO_3	$CHCl_3$	12

The optimized reaction conditions were used to carry out a total of fifteen reactions between three para substituted benzaldehydes viz. 4-chloro benzaldehyde, 4-bromo benzaldehyde, 4-nitrobenzaldehyde with a total of five different alcohols viz. methanol. ethanol, isopropanol, *tert*-butanol and benzyl alcohol. The yields of the corresponding esters obtained in these reactions are listed in (Table 3.4). The reactivity trend observed in **10** catalysed esterification of benzaldehyde with alcohol is comparable to those observed in the esterification reaction involving aryl boronic acid. The presence of strongly electron withdrawing group e.g. $–NO_2$ enhance the conversion whereas substrates containing poorly electron withdrawing group, 4-bromobenzaldehyde showed significantly lower yields. The electron withdrawing group at *p*-position significantly increases the electron density at the carbonyl carbon thus attack by the alcohol under basic condition become

more favourable. The reaction gives moderate to good yield for all the primary alcohols including the benzyl alcohol. Whereas, with *t*-BuOH low yield has been observed for all the substituted benzaldehydes and this can be possibly attributed to the relative steric bulkiness of the *tert*-butyl substituents.

Table 3.4. Optimization of esterification reaction of p-substituted benzaldehydes with different alcohols

Entry	Alcohol	X	% Yield
1	CH$_3$OH	-Cl	68
2		-Br	40
3		-NO$_2$	99
4	C$_2$H$_5$OH	-Cl	50
5		-Br	52
6		-NO$_2$	95
7	Isopropanol	-Cl	85
8		-Br	38
9		-NO$_2$	98
10	*tert*-BuOH	-Cl	60
11		-Br	29
12		-NO$_2$	72
13	Benzyl Alcohol	-Cl	92
14		-Br	25
15		-NO$_2$	99

The recyclability of the catalyst in both the esterification reactions were investigated by using *p*-chloro benzaldehyde as model substrate. After each successive catalytic run, **10** was recovered from the reaction mixture by centrifugation, washed several times with water and dried at 60 °C before using it in the next catalytic run. The catalyst maintained excellent efficiency in both the esterification reaction with no discernible loss up to 5th

catalytic run. The powder X-ray diffraction pattern and FT-IR spectra of the used catalyst after 6th cycle of the both the esterification reaction do not show any significant difference from those observed in case of a freshly prepared sample of **10** (Figure 3.14).
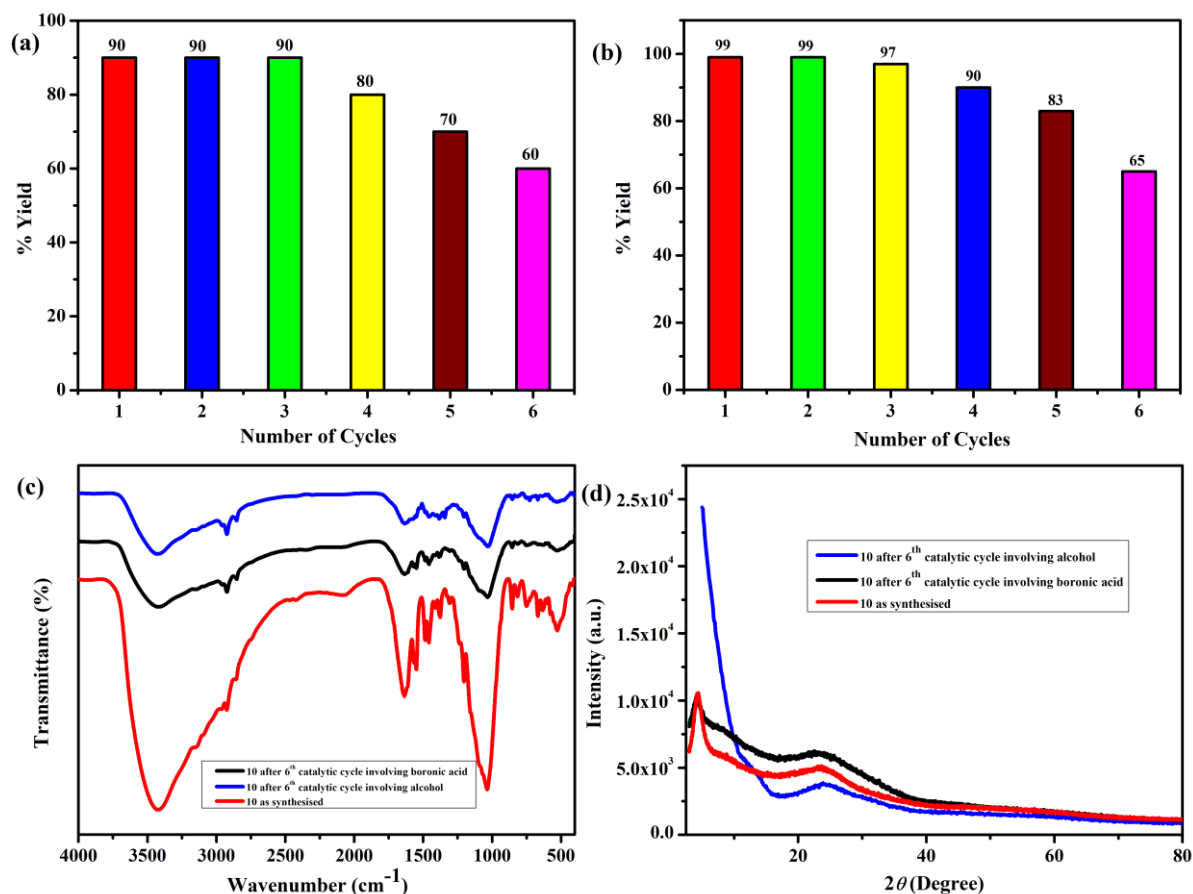

Figure 3.14. % yield of ester formed during six consecutive catalytic cycle of **10** catalysed esterification of benzaldehyde with (a) aryl boronic acid (b) methanol (c) FT-IR of as synthesised **10** and **10** isolated after 6th catalytic cycles (d) powder X-ray diffraction pattern of as synthesised **10** along with catalyst isolated after 6th catalytic cycle

3.5. Conclusions

Thus, a zirconium(IV) phosphoanate containing covalently anchored imidazolium functionality is prepared and characterized by using analytical, spectroscopic, structural and microscopic techniques. The synthetic procedure adopted for preparation of the imidazolium functionalized Zr(IV) phosphonate is simple and facile giving high yield. The catalytic efficacy of the imidazolium fucntionalized Zr(IV) phosphonate was examined in esterification reaction of benzaldehydes with either aryl boronic acid or alcohols. exhibits efficient catalytic activity with reusability upto 5 times without losing its efficiency.

3.6. References

[1]   Enders, D., Niemeier, O., and Henseler, A. Organocatalysis by N-heterocyclic carbenes. *Chemical Reviews*, 107(12):5606-5655, 2007.

[2]   Marion, N., Díez-González, S., and Nolan, S.P. N-heterocyclic carbenes as organocatalysts. *Angewandte Chemie International Edition*, 46(17):2988-3000, 2007.

[3]   Enders, D. and Balensiefer, T. Nucleophilic carbenes in asymmetric organocatalysis. *Accounts of chemical research*, 37(8):534-541, 2004.

[4]   Cazin, C.S. *N-Heterocyclic carbenes in transition metal catalysis and organocatalysis* . Springer Science & Business Media, 2010.

[5]   Díez-González, S., Spivey J. J., and Bertrand, G. Royal Society of Chemistry. London, 2011.

[6]   Flanigan, D.M., Romanov-Michailidis, F., White, N.A., and Rovis, T. Organocatalytic reactions enabled by N-heterocyclic carbenes. *Chemical Reviews*, 115(17):9307-9387, 2015.

[7]   Breslow, R. On the mechanism of thiamine action. IV. 1 Evidence from studies on model systems. *Journal of the American Chemical Society*, 80(14):3719-3726, 1958.

[8]   Bugaut, X. and Glorius, F. Organocatalytic umpolung: N-heterocyclic carbenes and beyond. *Chemical Society Reviews*, 41(9):3511-3522, 2012.

[9]   Harnying, W., Sudkaow, P., Biswas, A., and Berkessel, A. N-Heterocyclic Carbene/Carboxylic Acid Co-Catalysis Enables Oxidative Esterification of Demanding Aldehydes/Enals, at Low Catalyst Loading. *Angewandte Chemie International Edition*, 60(36):19631-19636, 2021.

[10]   Zhang, M., Zhang, S., Zhang, G., Chen, F., and Cheng, J. Palladium/NHC-catalyzed oxidative esterification of aldehydes with phenols. *Tetrahedron Letters*, 52(19):2480-2483, 2011.

[11] Delany, E.G., Fagan, C.L., Gundala, S., Mari, A., Broja, T., Zeitler, K., and Connon, S.J. NHC-catalysed aerobic aldehyde-esterifications with alcohols: no additives or cocatalysts required. *Chemical Communications*, 49(58):6510-6512, 2013.

[12] Reddy, R.S., Rosa, J.N., Veiros, L.F., Caddick, S., and Gois, P.M. NHC/Iron cooperative catalysis: aerobic oxidative esterification of aldehydes with phenols. *Organic & Biomolecular Chemistry*, 9(9):3126-3129, 2011.

[13] De Sarkar, S., Grimme, S., and Studer, A. NHC catalyzed oxidations of aldehydes to esters: chemoselective acylation of alcohols in presence of amines. *Journal of the American Chemical Society*, 132(4): 1190-1191, 2010.

[14] Rosa, J.N., Reddy, R.S., Candeias, N.R., Cal, P.M., and Gois, P.M. NHC− Iron-Catalyzed aerobic oxidative aromatic esterification of aldehydes using boronic acids. *Organic Letters*, 12(12):2686-2689, 2010.

[15] Delany, E.G., Fagan, C.L., Gundala, S., Zeitler, K., and Connon, S.J. Aerobic oxidation of NHC-catalysed aldehyde esterifications with alcohols: benzoin, not the Breslow intermediate, undergoes oxidation. *Chemical Communications*, 49(58):6513-6515, 2013.

[16] Maji, B., Vedachalan, S., Ge, X., Cai, S., and Liu, X.W. N-heterocyclic carbene-mediated oxidative esterification of aldehydes: ester formation and mechanistic studies. *The Journal of Organic Chemistry*, 76(9):3016-3023, 2011.

[17] Noonan, C., Baragwanath, L., and Connon, S.J. Nucleophilic carbene-catalysed oxidative esterification reactions. *Tetrahedron Letters*, 49(25):4003-4006, 2008.

[18] Tang, S., Yuan, J., Liu, C., and Lei, A. Direct oxidative esterification of alcohols. *Dalton Transactions*, 43(36):13460-13470, 2014.

[19] Khan, Z., Javed, F., Shamair, Z., Hafeez, A., Fazal, T., Aslam, A., Zimmerman, W.B., and Rehman, F. Current developments in esterification reaction: A review on process and parameters. *Journal of Industrial and Engineering Chemistry*, 103:80-101, 2021.

[20] Kiran, I.C., Lalwani, K., and Sudalai, A. N-Heterocyclic carbene catalyzed esterification of aromatic aldehydes with alcohols under aerobic conditions. *RSC advances*, 3(6):1695-1698, 2013.

[21] Ekoue-Kovi, K. and Wolf, C. One-pot oxidative esterification and amidation of aldehydes. *Chemistry–A European Journal*, 14(21):6302-6315, 2008.

[22] Gaspa, S., Porcheddu, A., and De Luca, L. Recent developments in oxidative esterification and amidation of aldehydes. *Tetrahedron Letters*, 57(31):3433-3440, 2016.

[23] Dzieszkowski, K. and Rafiński, Z. N-Heterocyclic Carbene Catalysis under Oxidizing Conditions. *Catalysts*, 8(11):549, 2018.

[24] Schlögl, R. Heterogeneous catalysis. *Angewandte Chemie International Edition*, 54(11):3465-3520, 2015.

[25] Barrett, A.G., Love, A.C., and Tedeschi, L. ROMPgel-supported thiazolium iodide: an efficient supported organic catalyst for parallel Stetter reactions. *Organic Letters*, 6(19):3377-3380, 2004.

[26] Storey, J.M. and Williamson, C. Imidazole based solid-supported catalysts for the benzoin condensation. *Tetrahedron letters*, 46(43):7337-7339, 2005.

[27] Tan, M., Zhang, Y., and Ying, J.Y. Hydrosilylation of Ketone and Imine over Poly-N-Heterocyclic Carbene Particles. *Advanced Synthesis & Catalysis*, 351(9):1390-1394, 2009.

[28] Motesharei, K. and Myles, D.C. Multistep synthesis on the surface of self-assembled thiolate monolayers on gold: probing the mechanism of the thiazolium-promoted acyloin condensation. *Journal of the American Chemical Society*, 119(28):6674-6675, 1997.

[29] Schilling Jr, C.L. and Mulvaney, J.E. Quaternization and catalytic activity of poly (vinylthiazoles). *Macromolecules*, 1(5):452-455, 1968.

[30] Tajima, H., Niitsu, T., Inoue, H., and Ito, M.M. Effects of thiazolium counter anion and reaction media on the activity of immobilized thiazolium catalyst. *Journal of chemical engineering of Japan*, 34(4):553-557, 2001.

[31] Yamashita, K., Osaki, T., Sasaki, K., Yokota, H., Oshima, N., Nango, M., and Tsuda, K. Acyloin condensation in aqueous system by durable polymer-supported thiazolium salt catalysts. Journal of Polymer Science Part A: *Polymer Chemistry*, 32(9):1711-1717, 1994.

[32] Faber, M.C., Van den Berg, H.J., Challa, G., and Pandit, U.K. Polymer-bound thiamine models. IV. A simple synthetic route to immobilize a thiazolium salt to macroreticular polystyrene resins via a dimethylene spacer. *Reactive Polymers*, 11:117-126, 1989.

[33] Yamashita, K., Tokuda, H., and Tsuda, K. Syntheses of new thiazolium salt polymers and their catalytic activities. *Journal of Polymer Science Part A: Polymer Chemistry*, 27(4):1333-1339, 1989.

[34] Van den Berg, H.J., Challa, G., and Pandit, U.K. Polymer-bound thiamine models. III. Influence of site isolation on the catalytic activity of polystyrene-bound thiazolium salts. *Reactive Polymers*, 11:101-116, 1989.

[35] Yamashita, K., Watanabe, J., Ikeda, R., Abe, D., and Tsuda, K. A holoenzyme model of thiamin dependent enzymes: polymer catalyst supported thiazolium salt. *Macromolecules*, 22(11):4392-4394, 1989.

[36] Yu, F.L., Zhang, R.L., Xie, C.X., and Yu, S.T. Synthesis of thermoregulated phase-separable triazolium ionic liquids catalysts and application for Stetter reaction. *Tetrahedron*, 66(47):9145-9150, 2010.

[37] Zhou, Z.Z., Ji, F.Q., Cao, M., and Yang, G.F. An efficient intramolecular Stetter reaction in room temperature ionic liquids promoted by microwave irradiation. *Advanced Synthesis & Catalysis*, 348(14):1826-1830, 2006.

[38] Ueno, A., Kayaki, Y., and Ikariya, T. Cycloaddition of tertiary aziridines and carbon dioxide using a recyclable organocatalyst, 1, 3-di-tert-butylimidazolium-2-carboxylate: straightforward access to 3-substituted 2-oxazolidones. *Green chemistry*, 15(2):425-430, 2013.

[39] Zeng, T., Song, G., and Li, C.J. Separation, recovery and reuse of N-heterocyclic carbene catalysts in transesterification reactions. *Chemical Communications*, (41):6249-6251, 2009.

[40] Pascanu, V., González, M. G., Inge, A, K., and Martín-Matute, B. Metal–organic frameworks as catalysts for organic synthesis: A critical perspective. *Journal of the American Chemical Society*, 141(18):7223-34, 2019.

[41] Ezugwu, C.I., Kabir, N.A., Yusubov, M., and Verpoort, F. Metal–organic frameworks containing N-heterocyclic carbenes and their precursors. *Coordination Chemistry Reviews*, 307:188-210, 2016.

[42] Tanabe, K.K. and Cohen, S.M. Postsynthetic modification of metal–organic frameworks—a progress report. *Chemical Society Reviews*, 40(2): 498-519, 2011.

[43] Dhakshinamoorthy, A., Asiri, A.M., and Garcia, H. Metal–organic frameworks catalyzed C–C and C–heteroatom coupling reactions. *Chemical Society Reviews*, 44(7):1922-1947, 2015.

[44] Huang, L., Wang, H., Chen, J., Wang, Z., Sun, J., Zhao, D., and Yan, Y. Synthesis, morphology control, and properties of porous metal–organic coordination polymers. *Microporous and mesoporous materials*, 58(2):105-114, 2003.

[45] Canivet, J., Fateeva, A., Guo, Y., Coasne, B., and Farrusseng, D. Water adsorption in MOFs: fundamentals and applications. *Chemical Society Reviews*, 43(16):5594-5617, 2014.

[46] Wang, C., Liu, X., Demir, N.K., Chen, J.P., and Li, K. Applications of water stable metal–organic frameworks. *Chemical Society Reviews*, 45(18):5107-5134, 2016.

[47] Gagnon, K.J., Perry, H.P., and Clearfield, A. Conventional and unconventional metal–organic frameworks based on phosphonate ligands: MOFs and UMOFs. *Chemical reviews*, 112(2):1034-1054, 2012.

[48] Yang, C.Y. and Clearfield, A. The preparation and ion-exchange properties of zirconium sulphophosphonates. *Reactive Polymers, Ion Exchangers, Sorbents*, 5(1):13-21, 1987.

[49] Bhattacharyya, B., Mishra, S., and Gogoi, N. Accessing cationic zirconium phosphonate nanosheets for anion exchange applications. *Inorganica Chimica Acta*, 531:120706, 2022.

[50] Chessa, S., Clayden, N.J., Bochmann, M., and Wright, J.A. α-Zirconium phosphonates: versatile supports for N-heterocyclic carbenes. *Chemical communications*, (7):797-799, 2009.

[51] Ruddlesden, A.J., Mewis, R.E., Green, G.G., Whitwood, A.C., and Duckett, S.B. Catalytic transfer of magnetism using a neutral iridium phenoxide complex. *Organometallics*, 34(12):2997-3006, 2015.

[52] Mehring, M., Schürmann, M., and Ludwig, R. tert-Butylphosphonic Acid: From the Bulk to the Gas Phase. *Chemistry–A European Journal*, 9(4):837-849, 2003.

[53] Maricq, M.M. and Waugh, J.S. NMR in rotating solids. *The Journal of Chemical Physics*, 70(7):3300-3316, 1979.